Cataract-associated connexin 46 mutation alters its interaction with calmodulin and function of hemichannels

Received for publication, December 7, 2017, and in revised form, December 29, 2017 Published, Papers in Press, January 3, 2018, DOI 10.1074/jbc.RA117.001348

Zhengping Hu[‡§1], Manuel A. Riquelme[‡1], Bin Wang[¶], Vladislav Bugay[¶], Robert Brenner[¶], Sumin Gu[‡], and Jean X. Jiang[‡2]

From the Departments of [‡]Biochemistry and Structural Biology and [¶]Cellular and Integrative Physiology, University of Texas Health Science Center, San Antonio, Texas 78229 and the [§]Second Xiangya Hospital, Central South University, Changsha 410011, China

Edited by Velia M. Fowler

Connexin channels help maintain eye lens homeostasis and transparency. The G143R missense substitution in connexin (Cx) 46 is associated with congenital Coppock cataracts; however, the underlying molecular mechanism is largely unknown. Here, we report that compared with WT Cx46, the G143R substitution abolishes hemichannel conductance in *Xenopus* oocytes and in HeLa cells. Moreover, this substitution is dominant-negative and inhibits conductance of WT Cx46. CD analysis indicated that the substitution greatly reduces the α-helical structure of the intracellular Cx46 loop domain. Protein pull-down assays and isothermal titration calorimetry revealed that this Cx46 domain directly interacts with calmodulin (CaM) in a Ca^{2+}-dependent fashion, an observation confirmed by immunofluorescent co-localization of Cx46 with CaM. Interestingly, the G143R substitution enhanced the Cx46–CaM interaction and attenuated its abolishment by Ca^{2+} depletion. Moreover, Cx46 increased dye influx, and the G143R substitution augmented this effect. Inhibition of Ca^{2+}-mediated CaM activation blocked hemichannel permeability. The membrane potential plays a crucial role in Cx46 membrane permeability. We found that the activity of hemichannels is detectable under rest and hyperpolarization conditions but is eliminated with depolarization. These results suggested that the G143R substitution impairs voltage-dependent electrical conductance and alters membrane permeability mediated by Cx46 hemichannels. The latter likely is caused by the substitution-induced structural changes of the intracellular loop domain associated with the increased interaction with CaM and reduced Ca^{2+} sensitivity. The data suggest that the G143R-induced enhancement of the CaM–Cx46 interaction results in altered hemichannel activities and might be related to cataract formation.

The lens is a clear part of the anterior eye that focuses light and images onto the retina. Cataracts, referring to the clouding of the lens, are responsible for 51% of world blindness according to World Health Organization data in 2010 (1). The lens has three main parts: the capsule, the epithelial layer in the anterior portion, and fiber cells, which comprise the bulk of lens (2). Lens fiber cells communicate to each other and to the surface of the lens by gap junction channels and hemichannels. These channels allow small molecules (<1.2 kDa) like ions, second messenger, and metabolites to pass through (3–5). The lens is an avascular organ and thus relies in part upon gap junction channels and hemichannels to maintain its metabolic homeostasis and transparency. Hemichannels, also called connexins, are undocked halves of gap junction channels that are composed of six connexin molecules. Connexins are a family of structurally related transmembrane proteins with 21 identified members in the human and 20 identified members in the mouse. Each connexin protein has four transmembrane domains, two extracellular loop domains, and an N-terminal domain that are all highly conserved between different connexin members. However, the intracellular loop and C-terminal domains are highly diverse among connexin subtypes (6, 7).

Three connexins are present in the lens: Cx43,[3] Cx46, and Cx50, of which Cx46 and Cx50 are predominantly expressed in the lens fibers. A large body of evidence has shown that connexin gene mutations (missense, nonsense, deletion, insertion, and frameshift) of Cx46 or Cx50 coding genes, GJA3 and GJA8, respectively, are a major cause of congenital cataracts (5, 8). Most of the connexin mutations associated with cataracts are located in transmembrane and extracellular loop domains, including over 40 cataract-associated mutations of Cx46. Interestingly, the missense mutation G143R is located in the intracellular loop (IL) domain of Cx46. This mutation was identified in a four-generation Chinese family with congenital Coppock cataracts (9). This is a special type of cataract in the posterior region of the lens between the nucleus and the posterior pole. Gly^{143} is a highly conserved amino acid residue across members of connexin family from various animal species. Our previous study has shown that the G143R mutation altered gap junction and hemichannel function, leading to decreased cell viability (10). Here, we identify that Gly^{143} is located in the calmodulin

This work was supported by National Institutes of Health Grant EY012085 (to J. X. J.), Welch Foundation Grant AQ-1507 (to J. X. J.), and National Science Foundation Grant 1456862 (to R. B.). The authors declare that they have no conflicts of interest with the contents of this article. The content is solely the responsibility of the authors and does not necessarily represent the official views of the National Institutes of Health.

This article contains Fig. S1–S3.

[1] These authors contributed equally to this work.

[2] To whom correspondence should be addressed: Dept. of Biochemistry and Structural Biology, University of Texas Health Science Center, 7703 Floyd Curl Dr., San Antonio, TX 78229-3900. Tel.: 210-562-4094; E-mail: jiangj@uthscsa.edu.

[3] The abbreviations used are: Cx, connexin; ITC, isothermal titration calorimetry; CaM, calmodulin; IL, intracellular loop; MT, mutant; C, control; Ni-NTA, nickel-nitrilotriacetic acid; TIRF, total internal reflection fluorescence; IPTG, isopropyl β-D-thiogalactopyranoside.

(CaM)-binding region of Cx46, and this mutation increases the interaction between Cx46 and CaM.

CaM is a ubiquitous, calcium-binding protein with various protein targets, allowing it to affect multiple cellular functions. It has four EF-hand Ca^{2+}-binding motifs in its N and C domains. CaM undergoes a large conformational change after binding to Ca^{2+}, which exposes hydrophobic patches, allowing binding to target proteins and initiating diverse downstream biological reactions. Connexins are also shown to associate with Ca^{2+}/CaM as a part of gap junction complex (11). Elevated intracellular Ca^{2+} concentration is long known to inhibit gap junction function in cardiac cells (12). In this study, we showed by CD analysis that α-helical structural content was greatly reduced in the IL domain of Cx46 with G143R mutation. This mutation abolished voltage activation of Cx46 hemichannel electrical conductance while increasing hemichannel dye influx. Interestingly, this mutation enhanced the binding affinity between CaM and IL domain of Cx46 and reduced Ca^{2+} dependence of the interaction. Enhancement of the interaction between CaM and Cx46 resulting in altered hemichannel activity might be an underlying mechanism associated with the formation of cataracts.

Results

G143R mutation abolishes voltage-dependent electrical conductance and inhibits WT Cx46 conductance in a dominant-negative manner

To test voltage-dependent hemichannel conductance by WT and G143R mutant of Cx46, membrane potential and transmembrane currents were measured in *Xenopus* oocytes injected with WT or mutant Cx46 cRNA or co-injected with both together. Comparable levels of expression of WT proteins, mutant proteins, or both together were detected by Western blotting analysis, whereas no expression of Cx46 was detected in non-injected oocytes (Fig. 1*A*). The resting membrane potentials of oocytes injected with WT and mutant Cx46 were more depolarized than those injected with water, indicating that WT and mutant Cx46 form permeable hemichannels (Fig. 1*B*). These data are consistent with previous publications from our and other labs showing leakage of hemichannels under resting membrane potential (10, 13, 14). In voltage clamp mode, the oocytes that express WT Cx46 hemichannels display large outward currents at positive potentials. The resting potentials of oocytes injected with G143R mutant RNA, however, were slightly hyperpolarized compared with those injected with WT Cx46 RNA, whereas their transmembrane currents were negligible compared with those injected with water. Oocytes co-expressing WT and mutant Cx46 displayed significantly lower current amplitude than those expressing WT Cx46 alone, suggesting that Cx46G143R mutant has a dominant-negative effect on forming functional hemichannels when co-expressed with WT Cx46 (Fig. 1*C*). The voltage–current relationship of *Xenopus* oocytes alone or expressing Cx46, Cx46G143R, or both together shows that G143R mutant inhibited the ionic conductance induced by voltage in a dominant-negative manner (Fig. 1*D*).

To dissect the effect of Cx46G143R on hemichannel gating in mammalian cells, we performed cell patch clamp to record whole-cell currents in HeLa cells expressing WT or G143R mutant (MT) of Cx46 (Fig. 2). We have previously shown that both WT and G143R mutant are localized on the cell surface in HeLa cells using cell surface biotinylation assay (10). Moreover, the amount of mutant is less on the cell surface than that of WT. Negative control (C) cells were recorded in HeLa cells transfected with empty vector. The currents were measured from a ramp voltage command of −110 to +110 mV in 8 s. Whole-cell current recorded in HeLa cells expressing WT Cx46 increased from 4 s compared with control cells with hardly detectable conductance, whereas HeLa cells expressing G143R mutant showed the similar non-detectable whole-cell patch clamp current as negative control cells (Fig. 2*A*). The peak amplitudes of outward and inward currents from C, WT, and mutant-expressing cells were also obtained; outward current peaks were much higher than inward peaks. The outward peak was significantly different between WT and C but not significantly different for inward peak, and there was no difference between C and mutant (Fig. 2*C*). This result showed an abolishment of hemichannel conductance in G143R mutant in HeLa cells.

G143R mutation alters α-helical structural content of Cx46 IL domain and its response to pH and Ca^{2+}

To understand the underlying molecular mechanism of this connexin mutation, we first determined the secondary structural changes caused by this mutation in the IL domain by using CD techniques. The secondary structure of the GST-fusion protein containing Cx46 IL domain of WT or G143R MT was determined using CD. Molar ellipticity of far UV CD spectra of purified GST protein and fusion proteins, WT, and MT of Cx46 IL domains was recorded at pH 6.5, 7, 7.5, and 8 (Fig. 3 and Fig. S1). GST protein did not contain any α-helical structure (Fig. S1). A typical α-helical structure characterized by two peaks at ~209 and ~222 nm was observed in the WT GST-Cx46 IL domain. However, the GST-Cx46G143R IL domain is loosely structured with a negative peak at 198 nm and a less notable broad curve at 210–220 nm (Fig. 3*A*). In comparison of molar ellipticity of CD spectra between the Cx46 IL domain of WT and mutant under various pH conditions at 208-nm wavelength, WT varied from −40 to −60 (deg cm^2 $dmol^{-1}$) and was responsive to pH with decreasing α-helical contents. Meanwhile, the spectra of MT remain at −20 (deg cm^2 $dmol^{-1}$) and unresponsive to pH changes (Fig. 3*A*, *right bottom panel*). These data indicate that G143R mutation reduces not only the α-helical content but also responsiveness of the IL domain to pH.

We further determined responses of WT and MT versions of Cx46 IL domain to various Ca^{2+} concentrations (0–2.5 mM) in PBS (pH 7.5; Fig. 3*B*). The α-helical content of WT Cx46 IL decreased with the increase of Ca^{2+} concentration, especially at a Ca^{2+} concentration at 0–0.5 mM. In contrast, the MT IL domain was less responsive to Ca^{2+}. Together, these results show that G143R decreases the α-helical content of the IL domain and appears to lose sensitivity to pH and Ca^{2+}.

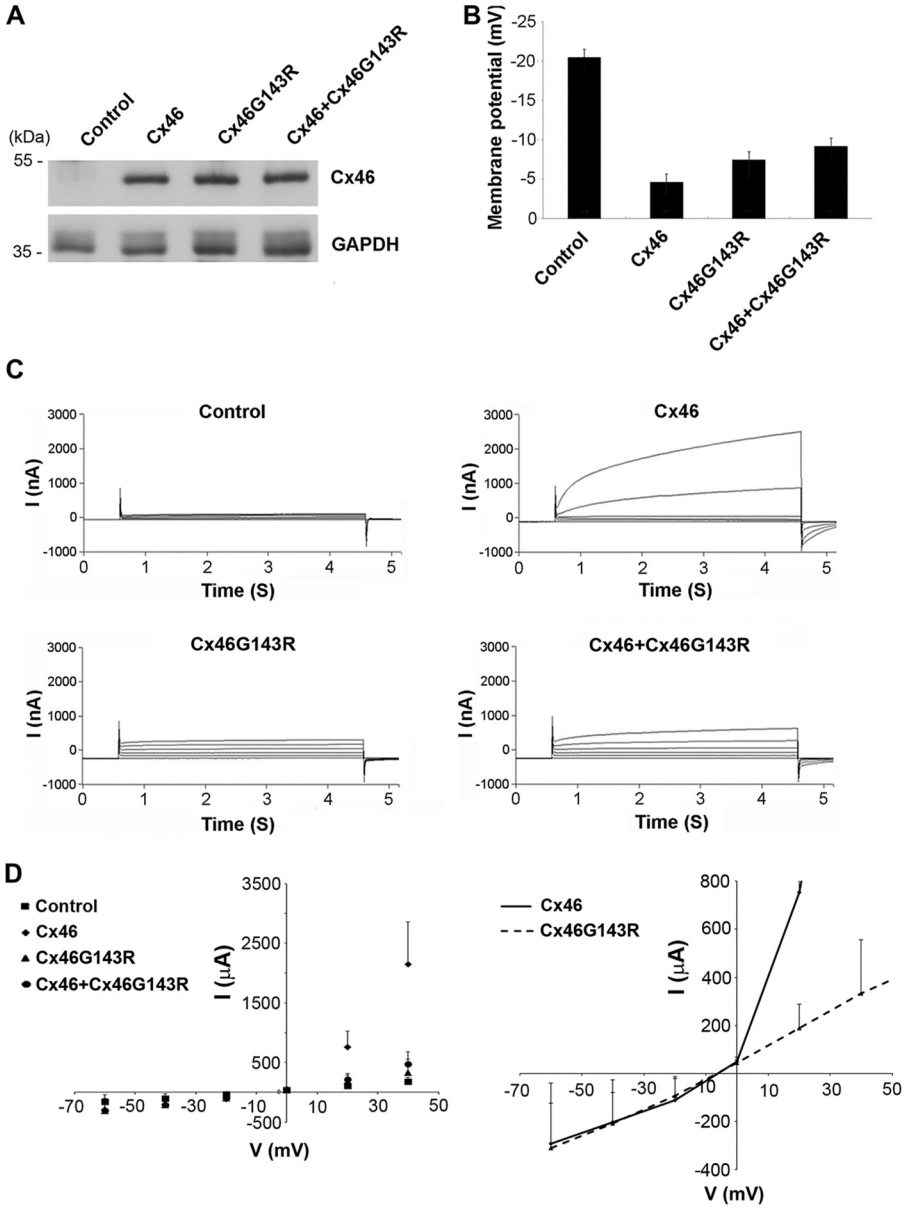

Figure 1. G143R mutant inhibits voltage gating of Cx46 and functions in a dominant-negative manner against WT Cx46. cRNA of Cx46 WT, G143R mutant, or both together were injected into *Xenopus* oocytes. *A*, membrane protein lysates of oocytes injected with cRNA of Cx46, Cx46G143R, and both together and H_2O-injected control were immunoblotted with anti-Cx46 antibody or anti-GAPDH antibody. *B*, resting membrane potential was measured in oocytes injected with H_2O or cRNA for Cx46, Cx46 G143R, or both together. *C*, voltage-dependent transmembrane current of oocytes was measured with voltage commands ranging from −60 to 40 mV. *D*, voltage–current relationship of *Xenopus* oocytes injected with H_2O or expressing Cx46, Cx46(G143R), or both together.

G143R mutant enhances the interaction between Cx46 IL domain and CaM

The G143R mutation is located in the CaM-binding pocket in the IL domain. CaM is known to influence gap junction channel gating (15). Protein pulldown assays were performed to determine the interaction between the Cx46 IL domain of WT or the G143R mutant with Ca^{2+}–CaM. Comparable levels of 7-His-tagged peptide containing Cx46 IL domain of WT or G143R mutant were immobilized on Ni-NTA beads (Fig. 4*A*, *lower panel*). Two concentrations of purified CaM protein, 1 and 3 μg, were incubated with a 7-His-WT or 7-His-G143R mutant fusion protein. More CaM was pulled down by Cx46 IL domain containing G143R mutation than WT with a minimal amount of CaM (Fig. 4*A*, *upper panel*). The co-immunoprecipitation data further confirmed the observation (Fig. 4*B*). Cx46 immunoprecipitated more CaM in cell lysates expressing mutant than WT proteins (Fig. 4*B*, *lower panel*, *IP: Cx46 Ab*), although cell lysates contained similar levels of Cx46 protein (Fig. 4*B*, *upper panel*, *Preload*). This result indicates that G143R mutant has a higher binding affinity with Ca^{2+}–CaM.

Isothermal titration calorimetry (ITC) experiments were performed to obtain the binding affinity and stoichiometry of the interaction between Cx46 IL domain and CaM (Fig. 5). We isolated His-tagged CaM and WT and mutant IL domains and determined their purity by SDS-PAGE (Fig. S2). The binding event is exothermic as predicted according to the interaction

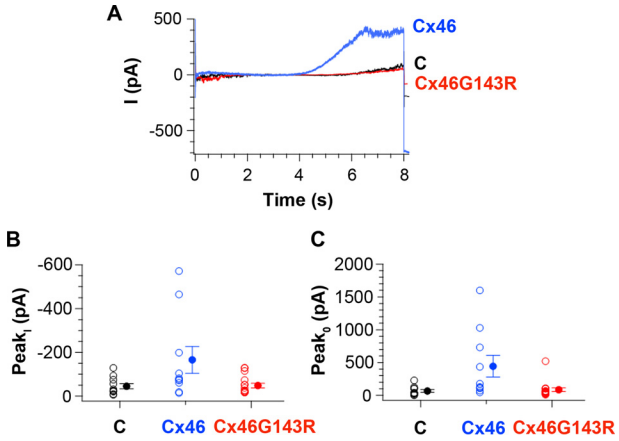

Figure 2. G143R mutant abolishes electrical conductance using whole-cell patch clamp recording of HeLa cells. *A*, representative whole-cell currents from cells transiently expressing WT or G143R mutant of Cx46. Negative control (*C*) was recorded from vehicle EGFP plasmid transfected cells. Voltage ramped from −110 to +110 mV in 8 s. *B* and *C*, peak amplitudes of inward and outward currents, respectively. The number of cells was 11, 10, and 16 for control, WT, and G143R mutant, respectively. WT is significantly different from G143R mutant (p values are 0.01 for both outward and inward peak). The outward peak is also significantly different between WT and control (p = 0.03), and the inward peak is not significantly different (p = 0.06). There are no differences between control and G143R mutant in both outward (p = 0.6) and inward peak (p = 0.8).

between Cx44 and CaM (16). In the presence of 2 mM Ca^{2+}, the dissociation constant of WT is 2.95 ± 1.5 μM, whereas K_d of the G143R mutant is 1.58 ± 0.7 μM (Fig. 5*A*). Moreover, both WT and G143R mutant bound to Ca^{2+}–CaM at ~1:1 ratio at pH 6.8, the physiological condition in the lens. The binding affinity for CaM is almost 2-fold higher in the mutant compared with WT. A similar difference in binding affinity between CaM and the IL domain of WT (2.5 μM) and mutant (1.17 μM) was observed with 0.3 mM Ca^{2+} (Fig. 5*B*). To determine whether this interaction occurs with active CaM, we conducted ITC in the absence of Ca^{2+} (EGTA-buffered solution). The interaction between WT IL domain and CaM did not happen without Ca^{2+}, whereas the interaction with CaM was still detectable with G143R mutant (Fig. 5*C*).

Confocal microscopy with immunolabeling of Cx46 and G143R showed a similar level of co-localization with CaM under normal extracellular Ca^{2+} conditions, and this co-localization was reduced in wildtype, but not in the mutant, under Ca^{2+}-depleted conditions (Fig. 6*A*). Because of the endogenous expression of CaM, we quantified the extent of co-localization by detecting the overlapping signals of Cx46 over CaM (Fig. 6*A*, *right panels*). Because antibody against extracellular domains of Cx46 is not available, fluorescent signals were generated from Cx46 on the plasma membrane as well as inside the cell. To validate the co-location results on plasma membrane, we used total internal reflection fluorescence (TIRF) microcopy that allows detection of proteins predominantly on plasma membrane (Fig. 6*B*). By quantification, a similar increased level of co-localization of MT was detected (Fig. 6*B*, *right panel*). For clear visualization, we presented individual staining with gray scale and merged in colors. Together, these data suggest that G143R mutation promotes the interaction between Cx46 and CaM, and this interaction even occurs without the activation of CaM by Ca^{2+}.

CaM regulates Cx46 hemichannel activity

We used a CaM inhibitor, calmidazolium chloride, to determine the role of CaM in Cx46 hemichannel activity. The rate of Etd dye uptake was greater in G143R mutant than in WT control. The dye uptake rate was greatly reduced in the presence of CaM inhibitor (Fig. 7*A*, *upper panel*, *Inh*). Ionomycin permits influx of Ca^{2+} through plasma membrane to raise intracellular level of Ca^{2+}. Application of ionomycin led to a dramatic increase in hemichannel uptake observed in both WT and G143R mutant as compared with non-treated controls (Fig. 7*A*, *lower left panel*). Moreover, this increased dye uptake by ionomycin was greatly reduced by the CaM inhibitor (Fig. 7*A*, *lower right panel*, *Inh*), suggesting that the increase in hemichannel activity was mediated by the activation of CaM via elevated intracellular Ca^{2+}. The rate of hemichannel dye uptake was quantified (Fig. 7*B*). A similar result was obtained with another hemichannel-permeable tracer, biocytin (Fig. 7*C*). In addition, HeLa cells alone (C) had minimal uptake. These results suggest that activated CaM is essential for the permeability of Cx46 hemichannels.

As shown in Fig. 1*B*, under resting membrane potential, WT and G143R Cx46 form leaky channels associated with the depolarization of plasma membrane. We examined the permeability of hemichannels under various membrane potentials by using Locke's saline buffer (resting potential) and varying extracellular Na^+ and K^+ concentrations (changing membrane potential) (Fig. 8 and Fig. S3). Increased permeability was observed for both WT and the mutant with 154 mM Na^+, a hyperpolarization condition. Additionally, hemichannel activity is even greater in G143R mutant than in WT (Fig. 8*A* and Fig. S3*A*). Replacing Na^+ with K^+ to depolarize cells did not enhance and even reduced permeability from that of resting potential. Depletion of extracellular Ca^{2+} is known to activate connexin hemichannels. However, the decreased activity of hemichannels under depolarizing conditions was also observed in the absence of extracellular Ca^{2+}, although the overall hemichannel activity is higher without extracellular Ca^{2+}. As shown in Fig. 7, Ca^{2+} influx at resting potential drastically increased hemichannel activity. Interestingly, this increase in hemichannel activity was not observed under depolarization conditions (Fig. 8*B* and Fig. S3*B*). To alleviate the possible influence of using positively charged molecule (Etd) on dye uptake, we conducted similar studies using biocytin, a neutral molecule. Similar to the observation with Etd (Fig. 8*A*), high extracellular Na^+ increased biocytin uptake in both WT and mutant, whereas high extracellular K^+ reduced biocytin uptake relative to levels at resting membrane potential (Fig. 8*C*). This result indicates that charges on tracer dye molecules are unlikely to be involved and supports a specific effect of membrane potential on hemichannel uptake. Together, the data suggest that membrane potential plays a critical role in Cx46 hemichannel activity; depolarization of membrane potential inactivates hemichannels. Under physiological membrane potential Ca^{2+}–CaM, possibly through the interaction with intracellular loop of Cx46, increases hemichannel activation. In contrast, the G143R mutation dysregulates and enhances the interaction with CaM,

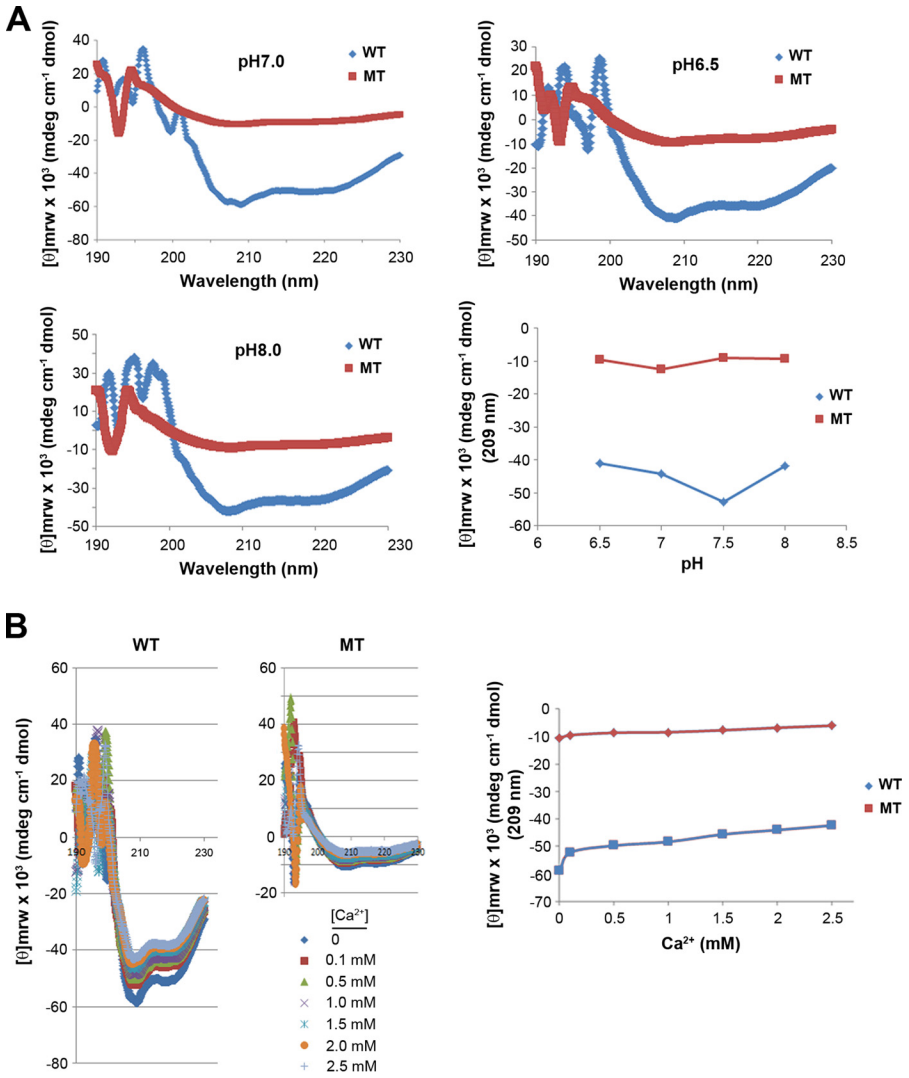

Figure 3. G143R mutation altered α-helical structural content of Cx46 IL domain and its responses to pH and Ca^{2+}. GST fusion protein containing Cx46 IL domain of WT or G143R MT was purified. *A*, molar ellipticity of far UV CD spectra of purified GST fusion proteins containing WT and MT of Cx46 IL domains were recorded at pH 6.5, 7, 7.5, and 8 at room temperature. WT shows a typical α-helical structure with two negative peaks at 209 and 222 nm. MT is less structured with a negative peak at 198 nm and a less noticeable broad curve at 210–220 nm. *B*, molar ellipticity of far UV CD spectra of WT and MT fusion proteins was recorded at pH 7.5 with Ca^{2+} at various concentrations (0–2.5 mM). With increased Ca^{2+} concentration, α-helical structural content is gradually reduced in WT Cx46 fusion protein.

resulting in aberrant Ca^{2+} sensitivity and increased activity of hemichannels.

Discussion

G143R is the only mutation identified in the IL domain region of Cx46 linking to congenital cataracts. Our earlier study showed that this mutation impairs gap junction channels while enhancing hemichannel activity as indicated by the dye uptake assay (10). This study aims to elucidate the underlying mechanism concerning how this mutation causes dysfunction of connexin hemichannels in the lens. Gly^{143} is a highly conserved amino acid residue across various types of connexins and animal species. Our CD study shows that the IL domain of Cx46 has considerable α-helical content that is sensitive to pH and Ca^{2+}. G143R, in which the small hydrophobic side chain of glycine is replaced with the large, positive charged one of asparagine, results in a great reduction in α-helical structural content of the IL domain. Moreover, this mutation renders the IL domain less sensitive to Ca^{2+} and pH. Inside human lens fiber cells, pH is relatively low (pH ~ 6.6) and Ca^{2+} is high (0.5–1 mM) (17). This lack of adaptability by the mutation to *in situ* physiological environment might partially be responsible for malfunction of channel activities. Elevation of intracellular Ca^{2+} concentration was long thought to be related to the reduction of permeability in gap junction channels (18). CaM was recognized to play a critical role in regulating gap junction channels by uncoupling gap junction channels and inhibiting gap junction permeability (19). Although extracellular Ca^{2+} inhibits hemichannel opening, intracellular Ca^{2+} is reported to positively regulate Cx43 and Cx32 hemichannel activity (20–22). Additionally, increased intracellular Ca^{2+} enhances the electrical conductance of Cx46 hemichannels, contrary to the reduced gap junction channels (20). Concurring with our finding, another paper reports that residue Gly^{45} in Cx26 is a Ca^{2+} sensor, and mutation of this residue to Glu in the keratitis–ichthyosis–deafness syndrome leads to "leaky" hemichannels and cell death (23).

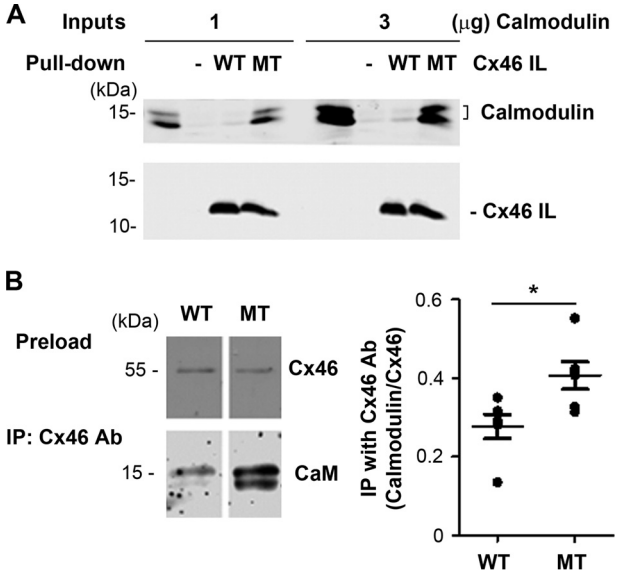

Figure 4. G143R mutant enhances the interaction between Cx46 IL domain and CaM. *A*, 7-His-linked peptide containing WT or G143R MT of Cx46 IL domain was purified. The protein pulldown assay was conducted with Ni-NTA beads. 1 or 3 μg of purified CaM protein was incubated with 7-His-linked WT or MT peptide and beads. The eluted fractions were immunoblotted with anti-His or anti-CaM antibody. *B*, co-immunoprecipitation assay was performed with lysates of cells expressing WT or mutant and anti-Cx46 antibody. Cx46 in the preloaded cell lysates were immunoblotted with anti-Cx46 antibody (*upper panels*). The immunoprecipitates (*IP*) were immunoblotted by anti-CaM antibody (*lower panels*). The band intensity was quantified (*lower right panel*; $n = 5$). The data are presented as means ± S.E. *, $p < 0.05$.

Residue Gly^{143} is located in the Ca^{2+}–CaM–binding motif, and this mutation is likely to affect the interaction between Cx46 and CaM. A previous study reports that CaM mediates the Ca^{2+}-dependent regulation of Cx44, the sheep ortholog of human Cx46 (16). Another study suggests that unlike other gap junction channels, gating of Cx46 hemichannels is not directly regulated by Ca^{2+} but is likely mediated by CaM (24). We showed the direct interaction between the Cx46 IL domain and CaM using both protein pulldown and ITC. Furthermore, the interaction between Cx46 IL domain and CaM occurs in a Ca^{2+}-dependent manner. Interestingly, this interaction is enhanced by the Gly^{143} mutation at both low and high concentrations of CaM. Protein pulldown assay showed that, in contrast to WT IL domain with minimal association with CaM, the G143R mutant strongly associated with CaM. We also confirmed the increased interaction between CaM and full-length Cx46G143R protein using co-immunoprecipitation assay. In addition to Cx44, several previous studies using various biochemical approaches have shown the binding between the IL domain of α-connexins, including Cx43 (25), Cx44 and Cx50 (26), and Ca^{2+}–CaM. We further determined thermodynamic parameters of the interaction between Cx46 IL domain and CaM by ITC. Our ITC data suggest that the interaction between CaM and Cx46 IL domain is both enthalpically and entropically favorable in the presence of Ca^{2+} and is primarily driven by enthalpic change. This result is similar to what has been reported for Cx44 (16). The IL domain with G143R mutation has a 2-fold increase in binding affinity as compared with WT. Interestingly, in the absence of Ca^{2+}, the interaction with CaM was only detected in the IL domain containing G143R mutation, not in WT Cx46. In accordance with this data, our localization study also showed, contrary to WT, that the mutation attenuated reduction of co-localization in response to Ca^{2+} depletion. We further showed that CaM inhibitor only inhibited dye uptake of the mutant but has minimal effect on WT. The reduction of dye uptake of the mutant by CaM inhibitor could be due to disruption of the interaction between mutant Cx46 and CaM, whereas such inhibitory effect may not be prominent for WT because of its minimal interaction with CaM. The aberrant enhancement of the interaction by G143R mutation with CaM and dysregulation of connexin hemichannels might contribute to hemostasis impairment and cataract formation in the lens.

It has been shown that α-helicity of the IL domain of connexins contributes to the binding of CaM and helps stabilize protein conformation (27). Surprisingly, α-helical content was greatly reduced in the IL domain containing G143R mutation despite tighter binding to CaM. The Gly-to-Arg mutation adds a positively charged residue in the conserved CaM-binding motif (28) of the IL domain. In this case, the electrostatic interaction is likely to play an important role in the interaction between Cx46 IL domain and CaM. Indeed, our ITC data also show that this interaction is primarily driven by an enthalpic change, meaning an electrostatic change. Previous papers suggest the electrostatic interactions between Cx44 (ovine ortholog of Cx46) and CaM (16, 27). The ITC experimental data demonstrated that the stoichiometry between Cx46MT and CaM is one to one, which is consistent with predicated interaction between Cx44 and CaM. Furthermore, in that paper, they titrated the interaction under different salt concentrations and pH values, and the 7results showed that that the binding affinity at pH values near the isoelectric points of CaM (4.2) or the Cx44 IL peptide (10.8) was drastically weakened. Therefore, we believe the electrostatic interaction is the major force responsible for this interaction. This mutant can even interact with CaM without Ca^{2+} activation of CaM, possibly because of an increase in overall positive charges of Cx46 IL domain. This result also agrees with the study by Chen *et al.* (29), which shows that several positively charged residues on Cx50 are important for Cx50–CaM interaction.

There are two possible models with regard to how Ca^{2+}–CaM and connexin interaction regulates connexin channel function: one is that the interaction with CaM directly regulates Cx32 gap junction channel gating (11), and the other suggests that Ca^{2+}–CaM–connexin complex formation may act on other signal pathways, such as protein kinase C (PKC) or inositol 1,4,5-trisphosphate (IP3) signaling mechanisms (30, 31). Based on our studies with the G143R mutant, our data support the first model implicating a direct regulation of connexin channels by CaM. CaM and connexins, such as Cx35, are reported to be co-localized as evidenced by immunostaining studies (32). Here we observed the co-localization of Cx46 and CaM in HeLa cells. In the absence of Ca^{2+}, this co-localization was compromised only in WT and not in mutated Cx46-expressed cells.

Interestingly, contrary to enhanced hemichannel mediated dye influx, this mutation completely diminished voltage-depen-

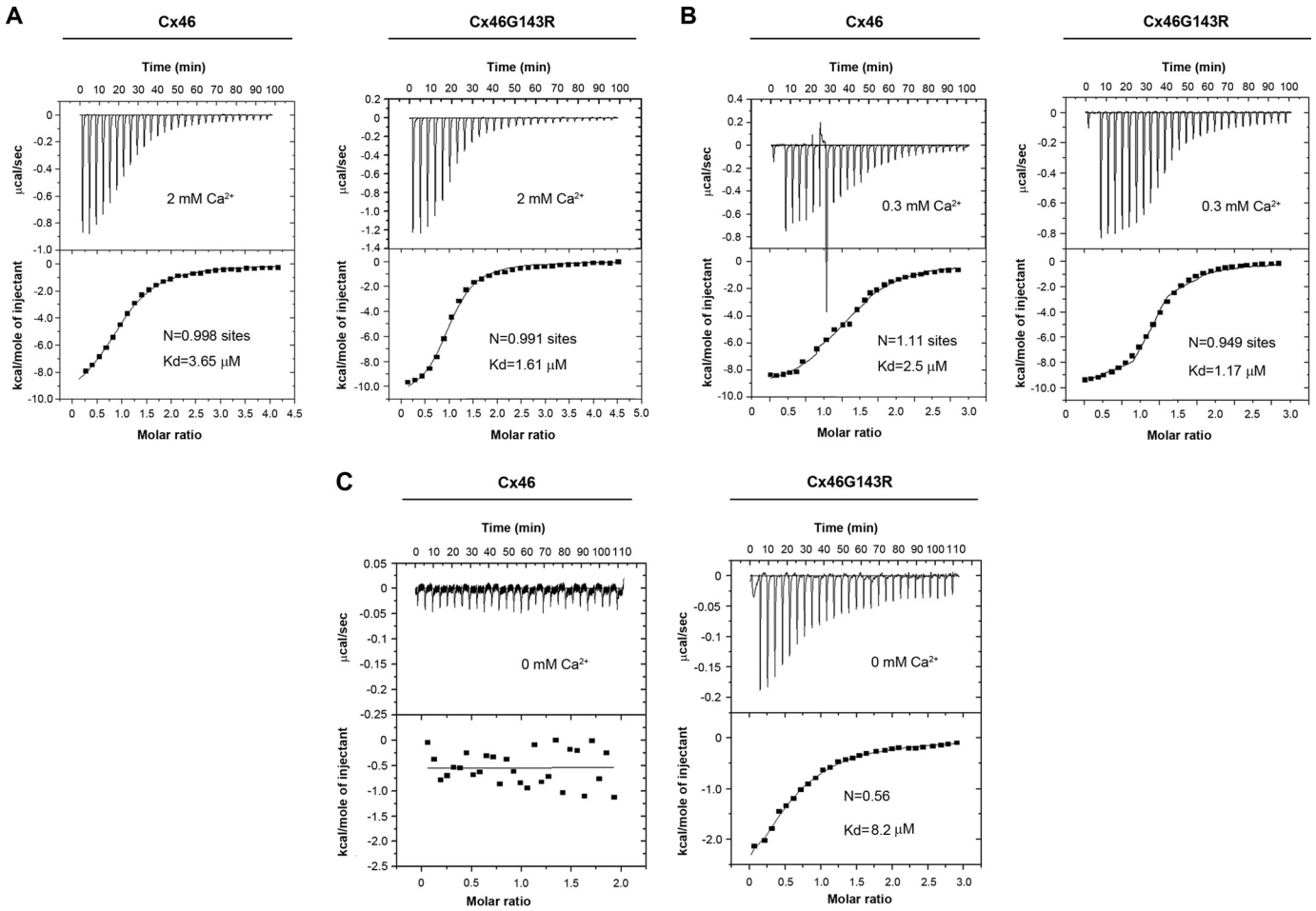

Figure 5. Cx46G143R mutation increases the binding affinity between Cx46 IL domain and CaM as evidenced by ITC. IL domain peptides of WT and mutant and CaM were generated. ITC microcalorimetric traces and derived isotherms of 20 μM CaM were titrated with 250 μM 7-His-tagged peptide containing WT or G146R mutant of Cx46 IL domain in the presence of 2 mM Ca^{2+} (*A*), 0.3 mM Ca^{2+} (*B*), and 0 mM Ca^{2+} (EGTA-buffered solution) (*C*). All the data were analyzed using Origin 7 software, and protein binding affinity (K_a) was determined. The binding stoichiometry between Cx46 IL domain and CaM is 1:1 ratio in the presence of Ca^{2+}. The G143R mutant shows increased binding affinity between Cx46 IL domain and CaM.

dent electrical conductance using both conductance measurement in *Xenopus* oocytes and whole-cell patch clamp in HeLa cells. Moreover, this mutant functioned in a dominant-negative manner by inhibiting the ion conductance by WT Cx46. This difference between gap junction channels and hemichannels in mediating transport of large molecules (*i.e.* dye molecules) and voltage-dependent electrical conductance has been reported (33, 34); however, the underlying mechanism remained largely obscure. Here, with the study of this mutation, we elucidated differential regulatory mechanisms with regard to hemichannel dye permeability under rest and depolarization membrane potential *versus* voltage-dependent gating of hemichannels.

Membrane potential appeared to play an essential role in hemichannel activity, and membrane depolarization completely compromised hemichannel activity even with the full activation of Ca^{2+}–CaM. However, under normal membrane potential, CaM activation by Ca^{2+} and binding to Cx46 are critical for hemichannel function. G143R mutation with aberrant CaM binding enhanced hemichannel activity only under normal membrane potential and not under depolarization conditions. This mutation instead totally lost voltage sensitivity compared with controls.

Two mechanisms have been proposed for voltage gating of gap junction channels: one is through conformational changes of a voltage sensor located in the N terminus, and the second is through the C terminus acting as a gating particle to block channel pore or stabilize the closed state (35). A recent study has shown that voltage dependence of the slow gate is located at charged residues of the first-transmembrane region of Cx46, as well as Cx26 and Cx50 (36). It is plausible that the mutation of Gly^{143} site may alter the conformation of the voltage sensor of Cx46, most likely through the interaction of C terminus, the second aforementioned mechanism. Our earlier study has shown that G143R mutation enhanced the interaction between IL domain and Cx46 molecule, and this interaction is likely to occur between IL and C terminus domains (10). Thus, C terminus may help stabilization of the closed state and also make a positive charge barrier that rectifies the positive ion flux. This mechanism is likely independent of the regulation of hemichannel dye permeability by Ca^{2+}–CaM. The summary of hemichannel behaviors of WT and G143R mutant under rest and hyperpolarization/depolarization membrane potentials is illustrated in Table 1.

Together, the study of this mutation helps uncover the differential regulatory mechanisms of connexin hemichannels in

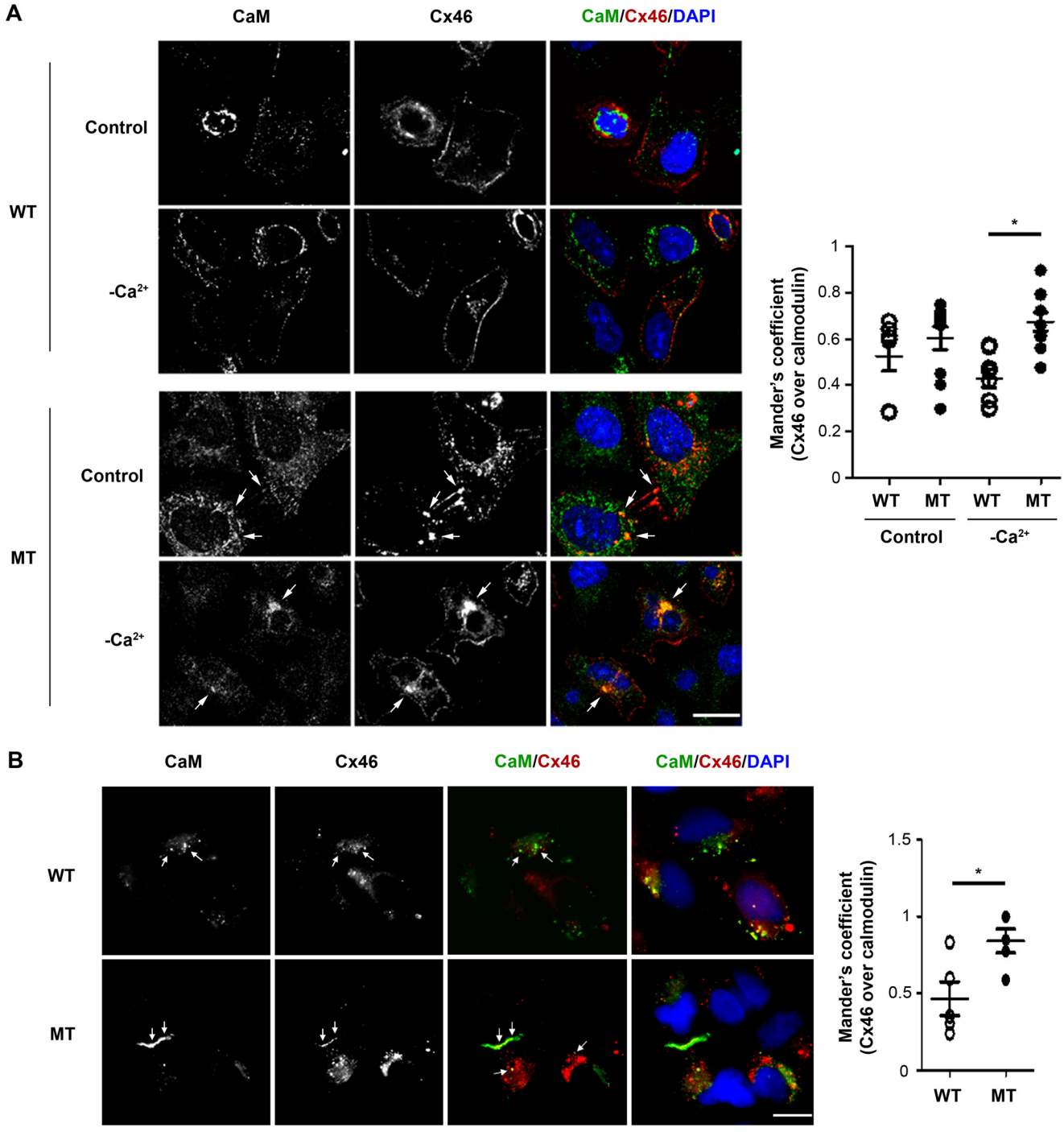

Figure 6. Co-localization of Cx46 and CaM was reduced by Ca^{2+} depletion only in WT and not in G143R-expressed cells. HeLa cells were transfected with WT and G143R mutant cDNAs, and 48 h after transfection, the cells were fixed and double immunolabeled with anti-Cx46 and anti-CaM antibodies. The co-localization was examined by confocal microscopy (*A*) and TIRF microscopy (*B*). The examples of co-localization signals were indicated (*white solid arrows*). The co-localization level of Cx46 over CaM signals was quantified using Mander's coefficient with ImageJ software (*right panels*). *Bar*, 20 μm. The data are presented as means ± S.E. *, $p < 0.05$.

membrane permeability by Ca^{2+}–CaM interactions and membrane potential and voltage-dependent gating of hemichannels. We showed that G143R mutation increased the interaction of CaM with Cx46 and altered dye permeability and electrical conductance. Cx46 channels are known to play an essential role in maintaining lens hemostasis, and recently more evidence indicates that connexin hemichannels may also be involved in transferring reductants. Moreover, the microcirculation model suggests that gap junction communication is a vital mechanism in excreting waste out of the lens (37). Therefore, the impairment of these channels could compromise cell protective function, and the molecular mechanism unveiled in our study could be related to the increased interaction with CaM in cataract lens because the Ca^{2+} level is much higher in cataract lens. Aberrant activities of Cx46 hemichannels with G143R mutation might lead to im-

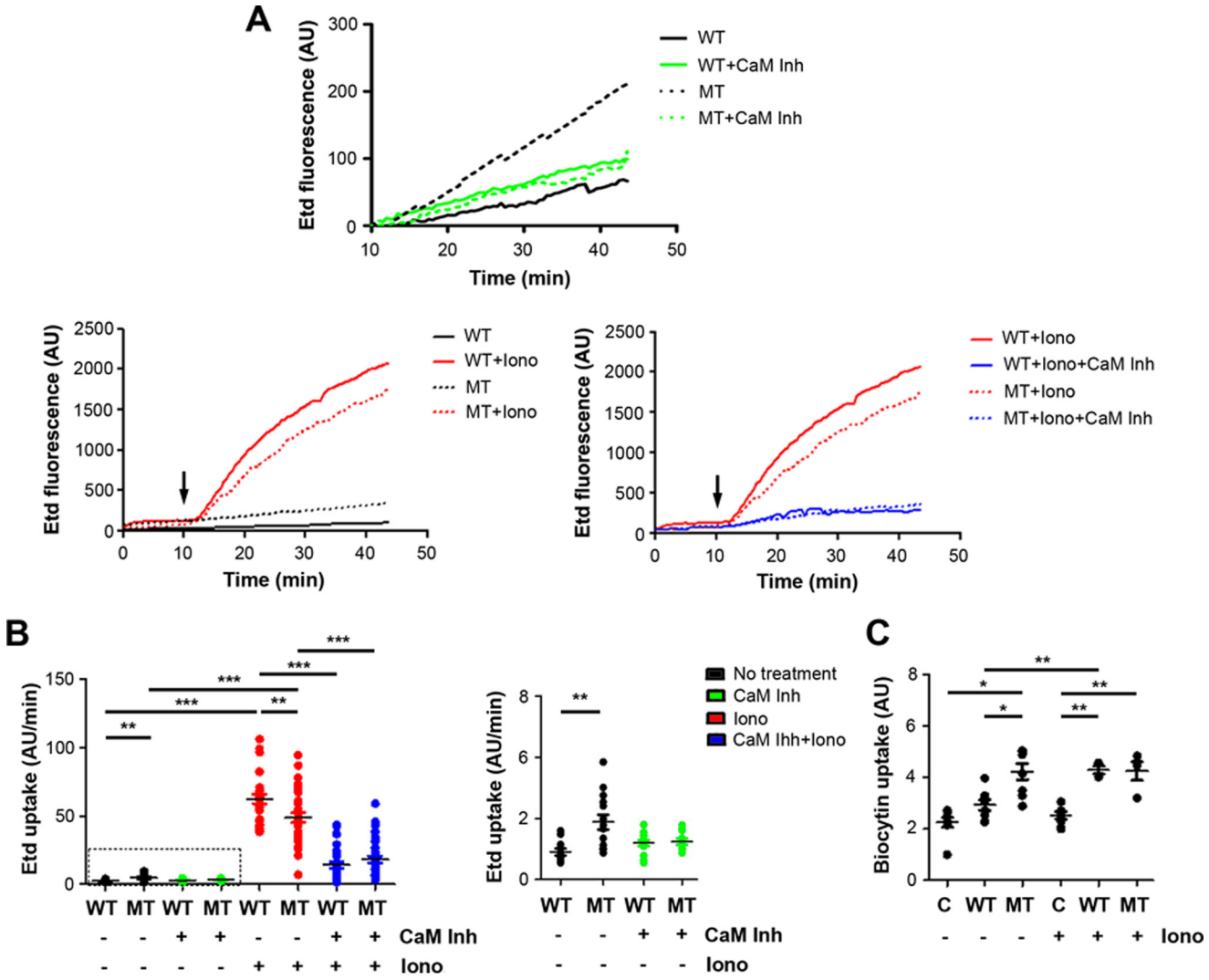

Figure 7. Hemichannel permeability depends on Ca^{2+}–CaM activation. HeLa cells were stably transfected with WT and G143R MT cDNAs. *A*, 48 h after transfection, the cells were pretreated with 10 μM CaM inhibitor (*Inh*, *green lines*) or calmidazolium for 30 min or treated with 2.5 μM ionomycin (*Iono*, *blue lines*) 10 min after application of Etd for up to 45 min. *Solid arrows* indicate the times when ionomycin was added. *B*, the rate of Etd dye uptake was measured and quantified by ImageJ software. The *dashed frame* was enlarged and is shown in the *right panel*. The data are presented as means ± S.E. *C*, biocytin dye uptake was performed in parental HeLa cells or HeLa cells stably transfected with WT or the MT with or without 2.5 μM ionomycin. *, $p < 0.05$; **, $p < 0.01$; ***, $p < 0.001$.

pairment of lens cell homeostasis and possibly cataract formation.

Experimental procedures

Materials

QIAquick® PCR purification kit, QIAquick® gel extraction kit, QIAprep® spin miniprep kit, and Ni-NTA-agarose beads were purchased from Qiagen. Paraformaldehyde was purchased from Electron Microscopy Science (Fort Washington, PA). Geneticin G418 was purchased from Life Technologies. Cell proliferation reagent WST-1 was purchased from Roche (Mannheim, Germany). Anti-human Cx46 antibody and anti-CaM antibody were purchased from Santa Cruz (Santa Cruz, CA). Phenyl Sepharose was purchased from GE Healthcare. All other chemicals were purchased from Sigma–Aldrich or Fisher Scientific unless it is specifically mentioned.

Plasmid constructs, Xenopus oocyte expression, and whole-cell electrical measurement

cDNAs for full-length human Cx46 and Cx46G143R mutant were subcloned into a pSP64T transcription vector as previously described (13). The constructs were confirmed by sequencing at the University of Texas Health Science Center at San Antonio DNA Sequencing Facility.

A 7-His-tagged protein containing the IL domain of human Cx46 was prepared. Briefly, a cDNA fragment encoding the IL domain of Cx46 (residues 98–152) was generated by PCR using Cx46 cDNA clone as a template with the following pair of primers: sense for WT IL domain, 5′-CATGCCATGGGCCACATCGTGCGCATGGAAGAGAAG-3′; antisense for WT IL domain, 5′-CGGGATCCTAATTAGTGATGATGATGATGATGATGGGTCCGCAGCAGCGCCCCGGCCATG-3′; sense for mutant IL domain: 5′-CATGCCATGGGCCACATCGTGCGCATGGAAGAGAAG-3′; and antisense for the IL domain

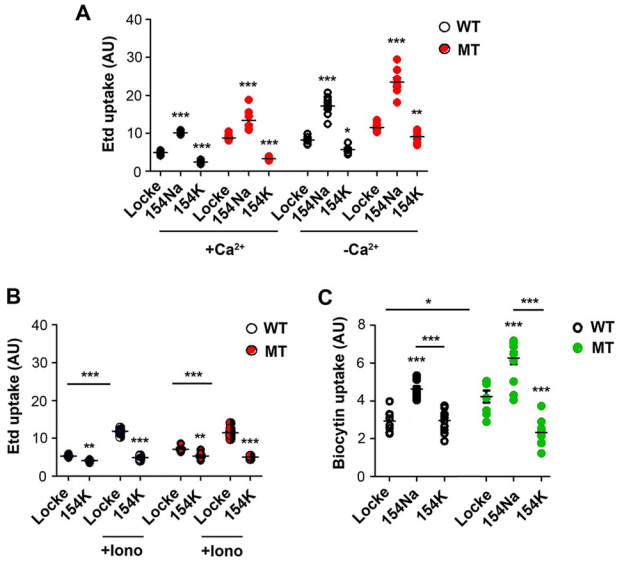

Figure 8. Membrane potential affects hemichannel permeability and it overrides Ca^{2+} sensitivity. HeLa cells were transfected with WT and G143R mutant cDNAs, and 48 h after transfection, the cells were incubated in Locke's saline or modified Locke's saline with extracellular 150 mM Na^+ or K^+. Etd dye uptake was performed in the absence or presence of extracellular 1.8 mM Ca^{2+} (*A*). The Etd dye uptake assay was conducted in the absence or presence of 2.5 μM ionomycin (*Iono*, *B*). Biocytin dye uptake was performed under extracellular 150 mM Na^+ or K^+ (*C*). As compared with corresponding rest membrane potential (Locke) in each group, *, $p < 0.05$; **, $p < 0.01$; ***, $p < 0.001$ (otherwise as indicated).

Table 1

Summary of hemichannel behaviors of WT and GIBR mutant under rest and hyper polarization/depolarization membrane potentials

WT	Physiological Ψm	+ Ψm	- Ψm
Plasma membrane permeability /High $[Ca^{2+}]_i$	↑	↓↓	↑
State of the Channel/High $[Ca^{2+}]_i$	Leaky/Open	Inactivated/ Inactivated	Leaky

G143R	Physiological Ψm	+ Ψm	- Ψm
Plasma membrane permeability/High $[Ca^{2+}]_i$	↑↑	↓↓	⇑
State of the Channel/High $[Ca^{2+}]_i$	Leaky/Open	Inactivated/ Inactivated	Leaky

harboring mutant, 5′-CGGGATCCTAATTAGTGATGATGATGATGATGATGGGTCCGCAGCAGCGCCCTGGCCATG-3′. The PCR DNA fragments were subcloned into the expression vector pET15b. The sequences of Cx46 WT and G143R mutant IL domains linked with 7-His were confirmed by sequencing.

In vitro transcription, Xenopus oocyte microinjection, and electrophysiological measurement

The pSP64T plasmid containing either full-length human Cx46 or Cx46G143R mutant were linearized with EcoRI and transcribed using the mMESSAGE mMACHINE *in vitro* transcription kit in accordance with the manufacturer's instructions. RNA concentration was estimated by non-denaturing gel electrophoresis with ethidium bromide staining. Diluted working solutions were prepared with RNase-free water and stored at −80 °C. Oocytes taken from ovarian lobe tissue of *Xenopus laevis* were defolliculated and microinjected with a 5-ng connexin cRNA along with 6 ng of Cx38 antisense RNA for endogenous Cx38 suppression (38). The oocytes were constantly incubated in half-strength L15 medium with 2 mM Ca^{2+} (Sigma) during the whole process. Two days after cRNAs injection, the oocytes were stripped of their vitelline membrane. A two-electrode voltage clamp method was used to measure the membrane potential and transmembrane current in *Xenopus* oocytes injected with WT or G143R mutant Cx46 cRNA. The solution in the electrode pipette contained 1.5 M KCl, 10 mM EGTA, and 10 mM HEPES as previously reported (39). In voltage-clamp mode, they displayed large outward currents when membrane potentials were depolarized to positive levels.

HeLa cells were bathed in normal Krebs solution to obtain the whole-cell recording configuration. Transfected Cx46 hemichannel currents became apparent after superfusing modified Krebs solution lacking calcium and containing 0.05 mM EGTA to buffer residual external calcium. The normal Krebs solution contained 140 mM NaCl, 4 mM KCl, 2 mM $CaCl_2$, 1 mM $MgCl_2$, 5 mM HEPES (pH 7.4), 5 mM glucose, and 2 mM pyruvate. Internal solution (patch pipette solution) was 120 mM potassium spartate, 10 mM NaCl, 1 mM $MgCl_2$, 3 mM MgATP, 5 mM HEPES (pH 7.2), and 2 mM EGTA filtered through a 0.22-μm membrane. Recordings were obtained using a HEKA EPC10 amplifier and Patchmaster software. The data were sampled at 10–30-μs intervals and low-pass filtered at 8.4 kHz using the HEKA EPC8 four-pole bessel filter. Voltage commands are described in the figure legends. Leak subtraction was not employed. Patch pipettes were pulled from Sutter Instruments borosilicate glass pipettes, were polished, and had a resistance of 3–5 MΩ in bath solution.

Expression and purification of fusion protein

7-His-tagged pET15b DNA constructs containing WT Cx46 IL domain or Cx46G143G mutant were transformed in BL21DE cells. 7-His-tagged peptides of WT and mutant were generated with IPTG induction and were affinity-purified by using Ni-NTA beads. The purified peptides were subject to 15% SDS-PAGE and immmunoblotted with anti-Cx46 or anti-His (1:1000 dilution) antibodies. CaM DNA construct in the pcDNA3.1 plasmid was a gift from Mark Shapiro (University of Texas Health Science Center). GST-Cx46 WT or GST-Cx46G143R IL domain fusion proteins were purified using glutathione beads. Fusion protein was dialyzed in PBS at pH 7.4 in 4 °C overnight. The CaM cDNA construct in PcDNA3.1 plasmid was transformed in BL21DE cells. CaM protein was induced by IPTG and purified using hydrophobic interaction chromatography with phenyl Sepharose (GE Healthcare). The purified CaM protein was subject to 15% SDS-PAGE and stained with Coomassie Blue.

CD measurements

Far-UV CD spectra (190–240 nm) with 60 nM CaM and 90 nM GST-Cx46 WT or GST-Cx46G143R IL domain fusion proteins were generated. Spectra were recorded on a Jasco-J-715 spectropolarimeter at room temperature and presented as CD absorption coefficient calculated on a mean residue weight basis. Under 0 mM Ca^{2+} condition, 1 mM EGTA was added to the solution.

Protein pulldown and immunoprecipitation assays

pET15b *Escherichia coli* containing 7-His-WT or G143R Cx46 IL domain was induced by IPTG, collected by centrifugation, and resuspended in lysis buffer (50 mM NaH_2PO_4, 300 mM NaCl, 10 mM imidazole, pH 8.0) with protease inhibitor (phenylmethanesulfonyl fluoride, leupeptin, and $NaVO_4$), sonicated, and centrifuged at 12,000 rpm for 30 min. The supernatant was mixed with Ni-NTA beads and incubated for 2 h at 4 °C, and the beads were washed twice with washing buffer (50 mM NaH_2PO_4, 300 mM NaCl, 40 mM imidazole, pH 8.0). Purified CaM was incubated with the beads attached with 7-His–linked WT or mutant attached Cx46 IL domain in binding buffer (20 mM HEPES, 100 mM KCl, 2 mM $CaCl_2$, pH 6.8) and incubated for 12 h at 4 °C. The beads were then washed with washing buffer twice, and elutes were analyzed on 15% SDS-PAGE and blotted with anti-CaM (1:1000 dilution) antibody. pET15b *E. coli* lysate incubated with Ni-NTA resin without 7-His-Cx46 WT or mutant IL was used as a negative control.

For co-immunoprecipitation studies, HeLa cells stably transfected with Cx46 or Cx46 G143R were collected with lysis buffer (20 mM HEPES, 100 mM KCl, 1 mM EDTA, pH 6.8) with protease and phosphatase inhibitor mixture. The cells were homogenized by passing 20 times through a 26-gauge needle. Then the cells were centrifuged at 5,000 × *g* for 10 min. The supernatants were collected, and crude membrane extracts were prepared. Briefly, the cell supernatants were ultracentrifuged to 100,000 × *g* for 40 min, and pellets were collected and resuspended in lysis buffer plus protease inhibitors. Membrane extracts were precleared by incubating with 10 μl of protein A/G-agarose (Santa Cruz) for 30 min followed by centrifugation at 7,000 × *g* for 5 min. The supernatants were collected and incubated with 600 ng of goat anti-Cx46 antibody (M-19) (Santa Cruz) and 0.1% BSA at 4 °C overnight and then were incubated with 20 μl of protein A/G-agarose (Santa Cruz) for 60 min. After incubation, the samples were centrifuged at 7,000 × *g* for 5 min and washed three times with lysis buffer plus protease and phosphatase inhibitors, 0.1% BSA 0.25% Triton X-100, and then were rinsed with PBS twice to remove BSA. The immunoprecipitates were eluted in non-reducing sample buffer and were analyzed by Western blotting analysis on 15% SDS-PAGE and immunoblotted with anti-CaM (1:1000 dilution) anti-Cx46 (1:500 dilution) antibody.

Isothermal titration calorimetry

ITC was performed with Cx46 7-His-Cx46 IL or 7-His Cx46(G143R) and CaM in 20 mM HEPES, 100 mM KCl, 2 mM $CaCl_2$ (pH 6.8) at 25 °C using the VP-ITC instrument (MicroCal, Northampton, MA). We added 1 mM EGTA to the solution to ensure 0 mM Ca^{2+} condition. All samples were degassed before the experiment. 250 μM 7-His-Cx46 IL or 7-His-Cx46G143R was placed in the syringe with 20 μM CaM in the cell. Cx46 IL peptides were titrated into the CaM solution at 6-min intervals with the first injection of 2 μl and the remaining 25 injections of 10 μl each. The titration was repeated three times. The data were analyzed using Origin 7 software. For each titration, the first 2-μl injection was ignored, the heat generated by dilution and mixing was subtracted, and fitting was done with the single binding site model. The parameters were obtained including stoichiometry (n), association constant (K_a), entropy (ΔS), and enthalpy change (ΔH). The binding constant (K_d) was generated from corresponding association constant (K_a).

Immunofluorescence co-localization analysis

HeLa cells cultured on glass coverslips were transfected with Cx46 or Cx46G14R cDNA using Lipofectamine transfection reagents. 48 h after the transfection, the cells were rinsed twice with DPBS and incubated in S-MEM in which 1.2 mM Ca^{2+} and 1 mM Mg^{2+} were added. Ca^{2+} depletion was performing by adding 1 mM EGTA, pH 7.4, and 10 μM thapsigargin for 30 min. The cells were then rinsed carefully twice with DPBS (Life Science) and fixed in cold 70% ethanol for 20 min at −20 °C. The cells were then blocked with 2% donkey serum, 1% BSA, and 1% fish gelatin for 1 h at room temperature and then incubated overnight at 4 °C with polyclonal goat anti-Cx46 antibody (1:500 dilutions) and mouse anti-CaM antibody (1:1000 dilution). The primary antibodies were detected by incubating with Alexa Fluro 594-conjugated donkey anti-goat secondary antibody (Life Science) for 1 h, rinsing three times with PBS, incubating with donkey anti-mouse Alexa 488 (Life Science), and then rinsing three times. Confocal fluorescence microscopy imaging was performed using a confocal laser scanning microscope (LSM710; Zeiss). Sequential laser scanning was conducted at a thickness of 1 μm. The images were deconvoluted using the ImageJ Iterative deconvolution plugin, with a known point spread function (for each image 20 iterations were applied with a low-pass filter diameter of 0.5 pixel). Brightness and contrast were adjusted off-line to improve clarity for each image. TIRF microscopy was conducted on a Nikon Eclipse TIRF system with an Ixon Ultra EMCCD camera (Andor Belfast, North Ireland). For this imaging modality, 60× TIRF objectives and #1 coverslips were used. To obtain the Mander's coefficient number, as an index of overlapping of pixels obtained from one channel over another channel (Cx46 over CaM signals), the ImageJ JACoP plugin was used.

Dye uptake assay

Hemichannel activity was measured using time-lapse measurements or snapshot photographs of dye uptake. HeLa cells stably transfected with Cx46 or Cx46G143R mutant were plated onto a 35-mm dish with recording medium (HCO_3-free αMEM medium buffered with 10 mM HEPES) containing 25 μM EtBr for time-lapse experiment. Some experiments were conducted in the presence of 2.5 μM ionomycin, which was added after 5 min, or 10 μM calmidazolium chloride, which was preincubated for 30 min before the recording. Fluorescence images were captured in a Nikon eclipse using a LASER-based

illumination system (MLC400B; Agilent, Santa Clara, CA), a rhodamine B filter, and an IXON3 EMCCD monochromatic digital camera (16-bit) (Andor, Belfast, UK) every 0.5 min. Image processing was performed off-line with ImageJ software (National Institutes of Health). The collected data were illustrated as pixel mean in arbitrary units per min.

For snapshot images, stably transfected HeLa cells were exposed to different Locke's saline solutions (154 mM NaCl, 5.4 mM KCl, 1.8 mM $CaCl_2$, 1 mM $MgCl_2$, 5 mM glucose, and 10 mM HEPES, pH 7.4) to manipulate the resting membrane potential. The change of composition was made using ion substitution by mixing different proportions of Locke's saline in which K^+ was substituted for Na^+. For zero Ca^{2+} and Mg^{2+} conditions, divalent cations were removed with 2.5 mM EGTA. Some experiments were conducted in the presence of 2.5 μM ionomycin, and this reagent was added to the recording medium with a constant presence of 50 μM of EtBr. The cells were exposed to EtBr for 15 min, rinsed three times with PBS, and fixed with 2% paraformaldehyde. For biocytin uptake, the cells were incubated in 250 μM biocytin in the different buffers for 20 min at room temperature and then rinsed with recording buffer and fixed with 4% paraformaldehyde for 10 min. The cells were then blocked with 2% goat serum, 1% BSA, and 1% fish gelatin for 1 h at room temperature and then incubated 1 h with polyclonal goat anti-biotin conjugated with rhodamine (1:500 dilutions). At least three microphotographs of fluorescence fields were taken with a 20× dry objective in an inverted microscope (Olympus, Tokyo, Japan) with a rhodamine filter. The image analysis was made offline with the ImageJ software. We measured the average of pixel density of 30 random cells.

Statistical analysis

All data were analyzed by GraphPad Prism 5 Software (GraphPad Software, La Jolla, CA). Two group comparisons were performed using paired design *t* test. Multiple group comparisons were conducted by one-way analysis of variance and Newmann–Keul's multiple comparison test. The data were presented as the means ± S.E. of at least three measurements. *p* values of less than 0.05 were designated as statistically significance differences. The *asterisks* in all figures indicate the degree of significance: *, $p < 0.05$; **, $p < 0.01$; and ***, $p < 0.001$.

Author contributions—Z. H., M. A. R., B. W., V. B., R. B., S. G., and J. X. J. conceptualization; Z. H., R. B., S. G., and J. X. J. resources; Z. H., M. A. R., B. W., V. B., R. B., S. G., and J. X. J. data curation; Z. H., M. A. R., B. W., V. B., R. B., S. G., and J. X. J. formal analysis; Z. H., R. B., S. G., and J. X. J. supervision; Z. H. and J. X. J. funding acquisition; Z. H., M. A. R., B. W., V. B., R. B., S. G., and J. X. J. validation; Z. H., M. A. R., B. W., V. B., R. B., S. G., and J. X. J. investigation; Z. H., M. A. R., B. W., V. B., R. B., S. G., and J. X. J. methodology; Z. H., M. A. R., B. W., V. B., R. B., S. G., and J. X. J. writing-original draft; Z. H. and J. X. J. project administration; and Z. H., M. A. R., B. W., V. B., R. B., S. G., and J. X. J. writing-review and editing.

Acknowledgments—We thank Drs. Eileen Lafer, Crystal Archer, and Chase Carver for technical assistance and Daniel Brian Shropshire for critical reading of the manuscript.

References

1. Pascolini, D., and Mariotti, S. P. (2012) Global estimates of visual impairment: 2010. *Br. J. Ophthalmol.* **96,** 614–618 CrossRef Medline
2. Forrester, J., Dick, A., Mcmenamin, P., and Lee, W. (1996) *The Eye: Basic Sciences in Practice*, W.B. Saunders Company Ltd., London
3. Mathias, R. T., White, T. W., and Gong, X. (2010) Lens gap junctions in growth, differentiation, and homeostasis. *Physiol. Rev.* **90,** 179–206 CrossRef Medline
4. Goodenough, D. A. (1992) The crystalline lens: a system networked by gap junctional intercellular communication. *Semin. Cell Biol.* **3,** 49–58 CrossRef Medline
5. Jiang, J. X. (2010) Gap junctions or hemichannel-dependent and independent roles of connexins in cataractogenesis and lens development. *Curr. Mol. Med* **10,** 851–863 CrossRef Medline
6. Goodenough, D. A., Goliger, J. A., and Paul, D. L. (1996) Connexins, connexons, and intercellular communication. *Annu. Rev. Biochem.* **65,** 475–502 CrossRef Medline
7. Meşe, G., Richard, G., and White, T. W. (2007) Gap junctions: basic structure and function. *J. Invest. Dermatol.* **127,** 2516–2524 CrossRef Medline
8. Gong, X., Cheng, C., and Xia C.-H. (2007) Connexins in lens development and cataractogenesis. *J. Membr. Biol* **218,** 9–12 CrossRef Medline
9. Zhang, L., Qu, X., Su, S., Guan, L., and Liu, P. (2012) A novel mutation in GJA3 associated with congenital Coppock-like cataract in a large Chinese family. *Mol. Vis.* **18,** 2114–2118 Medline
10. Ren, Q., Riquelme, M. A., Xu, J., Yan, X., Nicholson, B. J., Gu, S., and Jiang, J. X. (2013) Cataract-causing mutation of human connexin 46 impairs gap junction, but increases hemichannel function and cell death. *PLoS One* **8,** e74732 CrossRef Medline
11. Sotkis, A., Wang, X. G., Yasumura, T., Peracchia, L. L., Persechini, A., Rash, J. E., and Peracchia, C. (2001) Calmodulin colocalizes with connexins and plays a direct role in gap junction channel gating. *Cell Commun. Adhes.* **8,** 277–281 CrossRef Medline
12. Noma, A., and Tsuboi, N. (1987) Dependence of junctional conductance on proton, calcium and magnesium ions in cardiac paired cells of guinea-pig. *J. Physiol.* **382,** 193–211 CrossRef Medline
13. Paul, D. L., Ebihara, L., Takemoto, L. J., Swenson, K. I., and Goodenough, D. A. (1991) Connexin46, a novel lens gap junction protein, induces voltage-gated currents in nonjunctional plasma membrane of *Xenopus* oocytes. *J. Cell Biol.* **115,** 1077–1089 CrossRef Medline
14. Ebihara, L., Tong, J. J., Vertel, B., White, T. W., and Chen, T. L. (2011) Properties of connexin 46 hemichannels in dissociated lens fiber cells. *Invest. Ophthalmol. Vis. Sci.* **52,** 882–889 CrossRef Medline
15. Bennett, M. V., Barrio, L. C., Bargiello, T. A., Spray, D. C., Hertzberg, E., and Sáez, J. C. (1991) Gap junctions: new tools, new answers, new questions. *Neuron* **6,** 305–320 CrossRef Medline
16. Zhou, Y., Yang, W., Lurtz, M. M., Chen, Y., Jiang, J., Huang, Y., Louis, C. F., and Yang, J. J. (2009) Calmodulin mediates the Ca2+-dependent regulation of Cx44 gap junction. *Biophys. J.* **96,** 2832–2848 CrossRef Medline
17. Vanmarle, J., Jonges, R., Vrensen, G. F., and Dewolf, A. (1997) Calcium and its localization in human lens fibres: an electron tomographic study. *Exp. Eye Res.* **65,** 83–88 CrossRef Medline
18. Rose, B., Simpson, I., and Loewenstein, W. R. (1977) Calcium ion produces graded changes in permeability of membrane channels in cell junction. *Nature* **267,** 625–627 CrossRef Medline
19. Peracchia, C., Bernardini, G., and Peracchia, L. L. (1983) Is calmodulin involved in the regulation of gap junction permeability? *Pflugers Arch.* **399,** 152–154 CrossRef Medline
20. Figueroa, V., Sáez, P. J., Salas, J. D., Salas, D., Jara, O., Martínez, A. D., Sáez, J. C., and Retamal, M. A. (2013) Linoleic acid induces opening of connexin26 hemichannels through a PI3K/Akt/Ca^{2+}-dependent pathway. *Biochim. Biophys. Acta* **1828,** 1169–1179 CrossRef Medline
21. Wang, N., De Bock, M., Decrock, E., Bol, M., Gadicherla, A., Bultynck, G., and Leybaert, L. (2013) Connexin targeting peptides as inhibitors of voltage- and intracellular Ca^{2+}-triggered Cx43 hemichannel opening. *Neuropharmacology* **75,** 506–516 CrossRef Medline

22. De Vuyst, E., Decrock, E., Cabooter, L., Dubyak, G. R., Naus, C. C., Evans, W. H., and Leybaert, L. (2006) Intracellular calcium changes trigger connexin 32 hemichannel opening. *EMBO J.* **25,** 34–44 CrossRef Medline
23. Zhang, Y., and Hao, H. (2013) Conserved glycine at position 45 of major cochlear connexins constitutes a vital component of the Ca^{2+} sensor for gating of gap junction hemichannels. *Biochem. Biophys. Res. Commun.* **436,** 424–429 CrossRef Medline
24. Peracchia, C. (2004) Chemical gating of gap junction channels roles of calcium, pH and calmodulin. *Biochim. Biophys. Acta* **1662,** 61–80 CrossRef Medline
25. Zhou, Y., Yang, W., Lurtz, M. M., Ye, Y., Huang, Y., Lee, H. W., Chen, Y., Louis, C. F., and Yang, J. J. (2007) Identification of the calmodulin binding domain of connexin 43. *J. Biol. Chem.* **282,** 35005–35017 CrossRef Medline
26. Zhang, X., and Qi, Y. (2005) Role of intramolecular interaction in connexin50: mediating the Ca^{2+}-dependent binding of calmodulin to gap junction. *Arch. Biochem. Biophys.* **440,** 111–117 CrossRef Medline
27. Zou, J., Salarian, M., Chen, Y., Veenstra, R., Louis, C. F., and Yang, J. J. (2014) Gap junction regulation by calmodulin. *FEBS Lett.* **588,** 1430–1438 CrossRef Medline
28. Rhoads, A. R., and Friedberg, F. (1997) Sequence motifs for calmodulin recognition. *FASEB J.* **11,** 331–340 Medline
29. Chen, Y., Zhou, Y., Lin, X., Wong, H. C., Xu, Q., Jiang, J., Wang, S., Lurtz, M. M., Louis, C. F., Veenstra, R. D., and Yang, J. J. (2011) Molecular interaction and functional regulation of connexin50 gap junctions by calmodulin. *Biochem. J.* **435,** 711–722 CrossRef Medline
30. Billaud, M., Lohman, A. W., Johnstone, S. R., Biwer, L. A., Mutchler, S., and Isakson, B. E. (2014) Regulation of cellular communication by signaling microdomains in the blood vessel wall. *Pharmacol. Rev.* **66,** 513–569 CrossRef Medline
31. Retamal, M. A., Schalper, K. A., Shoji, K. F., Orellana, J. A., Bennett, M. V., and Sáez, J. C. (2007) Possible involvement of different connexin43 domains in plasma membrane permeabilization induced by ischemia-reperfusion. *J. Membr. Biol.* **218,** 49–63 CrossRef Medline
32. Flores, C. E., Cachope, R., Nannapaneni, S., Ene, S., Nairn, A. C., and Pereda, A. E. (2010) Variability of distribution of Ca^{2+}/calmodulin-dependent kinase II at mixed synapses on the mauthner cell: colocalization and association with connexin 35. *J. Neurosci.* **30,** 9488–9499 CrossRef Medline
33. Trexler, E. B., Bennett, M. V., Bargiello, T. A., and Verselis, V. K. (1996) Voltage gating and permeation in a gap junction hemichannel. *Proc. Natl. Acad. Sci. U.S.A.* **93,** 5836–5841 CrossRef Medline
34. Qu, Y., and Dahl, G. (2002) Function of the voltage gate of gap junction channels: selective exclusion of molecules. *Proc. Natl. Acad. Sci. U.S.A.* **99,** 697–702 CrossRef Medline
35. Bargiello, T. A., Tang, Q., Oh, S., and Kwon, T. (2012) Voltage-dependent conformational changes in connexin channels. *Biochim. Biophys. Acta* **1818,** 1807–1822 CrossRef Medline
36. Pinto, B. I., García, I. E., Pupo, A., Retamal, M. A., Martínez, A. D., Latorre, R., and González, C. (2016) Charged residues at the first transmembrane region contribute to the voltage dependence of the slow gate of connexins. *J. Biol. Chem.* **291,** 15740–15752 CrossRef Medline
37. Mathias, R. T., Kistler, J., and Donaldson, P. (2007) The lens circulation. *J. Membr. Biol.* **216,** 1–16 CrossRef Medline
38. Barrio, L. C., Suchyna, T., Bargiello, T., Xu, L. X., Roginski, R. S., Bennett, M. V., and Nicholson, B. J. (1991) Gap junctions formed by connexins 26 and 32 alone and in combination are differently affected by voltage. *Proc. Natl. Acad. Sci. U.S.A.* **88,** 8410–8414 CrossRef Medline
39. Ebihara, L., and Steiner, E. (1993) Properties of a nonjunctional current expressed from a rat connexin46 cDNA in *Xenopus* oocytes. *J. Gen. Physiol* **102,** 59–74 CrossRef Medline